Climate Dynamics (2005) 25: 461–476
DOI 10.1007/s00382-005-0036-1

Irene Fischer-Bruns · H. von Storch
J. F. González-Rouco · E. Zorita

Modelling the variability of midlatitude storm activity on decadal to century time scales

Received: 1 December 2004 / Accepted: 8 April 2005 / Published online: 12 August 2005

Abstract The output of several multi-century simulations with a coupled ocean–atmosphere general circulation model is examined with respect to the variability of global storm activity in winter on time scales of decades and longer. The frequency of maximum wind speed events within a grid box, using the lower limits on the Beaufort wind speed scale of 8 and 10 Bft as thresholds, is taken as the characteristic parameter. Two historical climate runs with time-dependent forcing of the last five centuries, one control simulation, and three climate change experiments are considered. The storm frequency shows no trend until recently. Global maps for the industrially influenced period hardly differ from pre-industrial maps, even though significant temperature anomalies temporarily emerge in the historical runs. Two indicators describing the frequency and the regional shift of storm activity are determined. In historical times they are decoupled from temperature. Variations in solar and volcanic forcing in the historical simulations as well as in greenhouse gas concentrations for the industrially influenced period are not related to variations in storm activity. Also, anomalous temperature regimes like the Late Maunder Minimum are not associated with systematic storm conditions. In the climate change experiments, a poleward shift of storm activity is found in all three storm track regions. Over the North Atlantic and Southern Ocean, storm activity increases, while it decreases over the Pacific Ocean. In contrast to the historical runs, and with the exception of the North Pacific storm frequency index, the storm indices parallel the development of temperature, exceeding the 2 σ-range of pre-industrial variations in the early twenty-first century.

I. Fischer-Bruns (✉)
Max-Planck-Institute for Meteorology, Hamburg, Germany
E-mail: fischer-bruns@dkrz.de
Tel.: +49-40-41173242
Fax: +49-40-41173298

H. von Storch · E. Zorita
Institute for Coastal Research, GKSS Research Centre, Geesthacht, Germany

H. von Storch
Meteorological Institute, University of Hamburg, Germany

J. F. González-Rouco
Dpt. Astrofisica y CC. Atmósfera,
Universidad Complutense de Madrid, Spain

1 Introduction

Storms, or more precisely, windstorms, are a characteristic of the maritime weather at mid-latitudes. They are responsible for a significant part of the rainfall, serious hazards both on land and at sea, mixing the ocean and efficiently transporting energy and substances. As such, storms deserve our attention. The formation of these baroclinic storms has long been disentangled since the days of Vilhelm Bjerknes (Friedman 1989), but knowledge about the statistics of storm events and their changes through time is limited.

It is particularly difficult to homogeneously "measure" storm intensities. The World Meteorological Organization (WMO) Beaufort scale is certainly the most useful, but records based on visual observations depend on subjective decisions as well as ship routing and other non-meteorological phenomena. Long series of direct wind observations almost always suffer from inhomogeneities. Proxies, in particular based on pressure readings, allow some reconstructions of past storm conditions (Schmidt and von Storch 1993; WASA 1998; Kaas et al. 1998; Alexandersson et al. 2000). Seemingly, the storm climate in Northern Europe and in the adjacent North Atlantic region has been relatively stable during the last 100 or even 200 years, even if some interdecadal variability prevails (Bärring and von Storch 2004). This view is supported

by scant historical evidence based on dyke repair costs in the seventeenth century (de Kraker 1999). This relative stability is astounding insofar as it contradicts the views of many people who, in history, have often perceived storms as having become more severe (von Storch and Stehr 2000).

From indirect evidence, in particular proxy data like tree ring width, it is known that the climate in historical times has undergone significant variations—with extended periods like the Little Ice Age and the Medieval Warm Period or shorter interruptions like the Late Maunder Minimum (1675–1710; Lamb 1977). The spatial extent of these episodes is subject to debate, but there is little doubt that significant temperature deviations prevailed during these times, over large areas. Our question is: Are these temperature variations associated with significant changes of storminess?

As already outlined, we cannot test this hypothesis—"significant temperature variations are linked to significant changes of storminess"—with observed or indirect data. Therefore, we resort to the output of several multi-centennial simulations with a climate model, forced realistically with variable solar output, effect of volcanic aerosols and greenhouse gases (GHGs) (González-Rouco et al. 2003; Zorita et al. 2004). Two of these runs simulate historical conditions in 1500–1990 and 1000–1990. They exhibit the above-mentioned historical temperature anomalies although the simulated anomalies are larger than the temperature anomalies estimated from proxy data and historical accounts (e.g. Mann et al. 1998). On the other hand, evidence is accumulating that the last-mentioned reconstructions underestimate variability on multi-decadal and centennial time scales (von Storch et al. 2004). Also, the temperatures during the Late Maunder Minimum period in the model are consistent with many local data (Zinke et al. 2004; Zorita et al. 2004). But even if the temperature variations in our model simulations were too large, this would not be a severe limitation for our attempt to test the hypothesis about a link between storminess and temperature variations. In the remainder of this paper we demonstrate that we have to reject the hypothesis and to conclude that mid-latitude storm activity is mostly decoupled from hemispheric temperature variations—even if the temperature variations are possibly too large. For the future scenario runs, however, we show that storm activity mostly parallels the development of temperature.

The paper is organized as follows: First, in Sect. 2, the model and experiments are described. In Sect. 3, our technique for determining storminess from wind speed data is explained. The frequency of storm days in terms of a storm frequency index is determined in Sect. 4. In Sect. 5 a storm shift index is introduced in order to ascertain the dominant modes of storm variability. The paper is concluded in Sect. 6 with a discussion.

2 Model and experiments

For all analyses we use the output of the coupled global Ocean-Atmosphere General Circulation Model ECHAM4/HOPE-G. The spectral expansion of T30 in the atmospheric model corresponds to a horizontal gridding of about 3.75°×3.75°. In the vertical, the model resolves 19 atmospheric layers. The global general circulation model of the ocean, HOPE-G, has a horizontal gridding of 2.8°×2.8°, refining to 0.5° near the equator, and 20 vertical levels. An annual mean flux correction of the heat and freshwater fluxes has been applied to the coupling between the ocean and the atmosphere component to remove the climate drift. The coupled model with its components has been documented in several publications, giving further details (Roeckner et al. 1992; Roeckner et al. 1996; Wolff et al. 1997; Legutke and Maier-Raimer 1999; Legutke and Voss 1999). The spatial resolution of T30 in ECHAM4 is sufficient for the representation of synoptic cyclones (Stendel and Roeckner 1998; Raible and Blender 2004). Since Stendel and Roeckner (1998) have shown that the storm tracks show satisfactory agreement when compared with ERA-15/ECMWF re-analysis data (deviations below 10%), we consider the model also as being suitable for our study.

Six climate simulations with different forcings are considered in this study: two realizations of a historic climate change simulation, three transient climate change experiments with idealized forcing simulating a future climate state, and a control simulation.

2.1 Historical simulations H1 and H2

The two historical climate simulations (González-Rouco et al. 2003; Zorita et al. 2004; von Storch et al. 2004) cover the periods 1500–1990 and 1000–1990. The time-dependent external forcing of the model has been determined according to estimates of changes in solar radiation, and volcanic and GHG forcing (carbon dioxide, methane and nitrous oxide). The solar and volcanic forcing has been derived from data that Crowley (2000) applied in his experiments. The historical simulations are referred to as H1 (1500–1990) and H2 (1000–1990). In this study only the years 1550–1990 of both runs are considered (in H1 the model achieves a stable state around year 1550).

2.2 Increased CO_2 integration CMIP2

During the Coupled Model Intercomparison Project (CMIP) exercise, the so-called extended CMIP2 experiment has been performed with ECHAM4/HOPE-G along with several other climate models (Meehl et al. 2000). The integration has been started from a control state (1990 conditions: CO_2 content of 353 ppm) with the CO_2 concentration of the model's atmosphere

increasing at a rate of 1% p.a. to quadrupling (140 years). This concentration has then been held constant until simulation year 152. The 1% p.a. increase represents changes in equivalent CO_2 concentration, describing the radiative effects of the major GHGs, which are well mixed throughout the atmosphere. This climate change experiment is referred to as CMIP2 in this study.

2.3 Increased CO_2 integrations A2 and B2

The Special Report on Emissions Scenarios (SRES; Nakicenovic and Swart 2000) describes a set of emissions scenarios used in the Intergovernmental Panel on Climate Change (IPCC) Third Assessment Report. These scenarios have been designed to investigate future changes in the global environment especially taking into account the release of greenhouse gases and aerosol precursor emissions.

We consider results of the model driven by a forcing prescribed by the IPCC SRES A2 and B2 emissions marker scenarios for CO_2 and CH_4 (with no aerosol changes). The main scenario characteristic of A2 is a very heterogeneous world with a continuously increasing population, strengthened regional cultural identities and slow economic development. B2 assumes a slower population growth with intermediate levels of economic development and more accent on environmental protection resulting in lower emissions and less future warming than A2 (for more details see Nakicenovic and Swart 2000). We refer to these climate change experiments as A2 and B2.

2.4 Control integration N

For the control simulation, the climate model has been integrated for 1,000 years with fixed solar and GHG forcing corresponding to present-day conditions (forcing values: solar (1,365 Wm^{-2}), GHG concentrations: CO_2 (353 ppm), CH_4 (1,720 ppb), N_2O (310 ppb)). The control run simulates a realistic contemporary climate (Min et al. 2004). This experiment is referred to as N hereinafter.

3 Evidence for storminess based on near-surface wind speed data

For the assessment of extreme wind speed events long time series of simulated maximum 10 m wind speed are analyzed. Following the concept of Weisse et al. (2005), we investigate the near-surface wind speed data directly instead of analyzing proxies for storminess (e.g. cyclone counts based on surface pressure). This approach has been chosen in order to avoid assumptions to be made when using tracking algorithms. It is also reasonable since the wind speed data are easily accessible in a high temporal resolution. They are stored by the model every 30 min, compared internally with the preceding value and output every 12 h. At every grid point we then determine the maximum value for each day.

As thresholds for extreme wind speed events, the two lower limits (17.2 ms^{-1} and 24.5 ms^{-1}) on the WMO Beaufort wind speed scale of 8 Bft (17.2–20.7 ms^{-1}) and 10 Bft (24.5–28.4 ms^{-1}) are selected. A 'storm day' (in our notation) is counted if the daily near-surface maximum wind speed reaches or exceeds the threshold of 8 Bft. Thus, the total mean number of storm days per season is given by the mean number of days when the maximum wind speed reaches at least 8 Bft. If the threshold of 10 Bft is reached or exceeded, the day is classified as a 'severe storm day'. We only consider northern and southern winter (DJF and JJA) since, in general, the winter has more intense extra-tropical storms.

4 Frequency of storm days—storm frequency index

With respect to maximum 10 m wind speed we investigate first the frequency of storm days for the pre-industrial time period from 1551 to 1850 in the simulations H1 and H2. Global maps for the total mean number of storm days per season exhibit the well-known storm tracks in the NH for the northern winter season (DJF) and in the SH for the southern winter season (JJA) (Fig. 1a, b, shown for H2). NH and SH stand for northern and southern hemispheres respectively in the following. ''Hemispheric means'' refer to spatial averages from 90 N–15 N and 90 S–15 S, respectively. The largest frequency of extra-tropical storms in DJF can be seen to occur in the central North Atlantic and central North Pacific Ocean, to the east of the paths of relatively warm ocean currents that follow the eastern seaboards of North America and Asia, moving poleward and creating large temperature contrasts with the cold continents. In these areas of large temperature gradients and thus large vertical wind shear, the baroclinic disturbances draw energy from the mean flow, which is required for generating and strengthening storm systems. Another storm track circumnavigates the cold continent of Antarctica (JJA). In the Mediterranean region the frequency of storm days is low (Fig. 1a). As extreme wind speed events are produced by strong pressure gradients associated with cyclones, we suppose an underestimation of the number of cyclones in this area. Since Mediterranean cyclones are generally quite shallow and relatively small in scale, they are not well represented by this model version having the relatively coarse resolution of T30. Also, this region appears to be dependent more on local processes than on the North Atlantic storm track (Knippertz et al. 2003).

In the storm track regions the mean number of storm days per season is about 50–60 out of 90 days. The mean number of severe storm days only amounts to 10–20 per season (not shown). Hence, in the following we focus

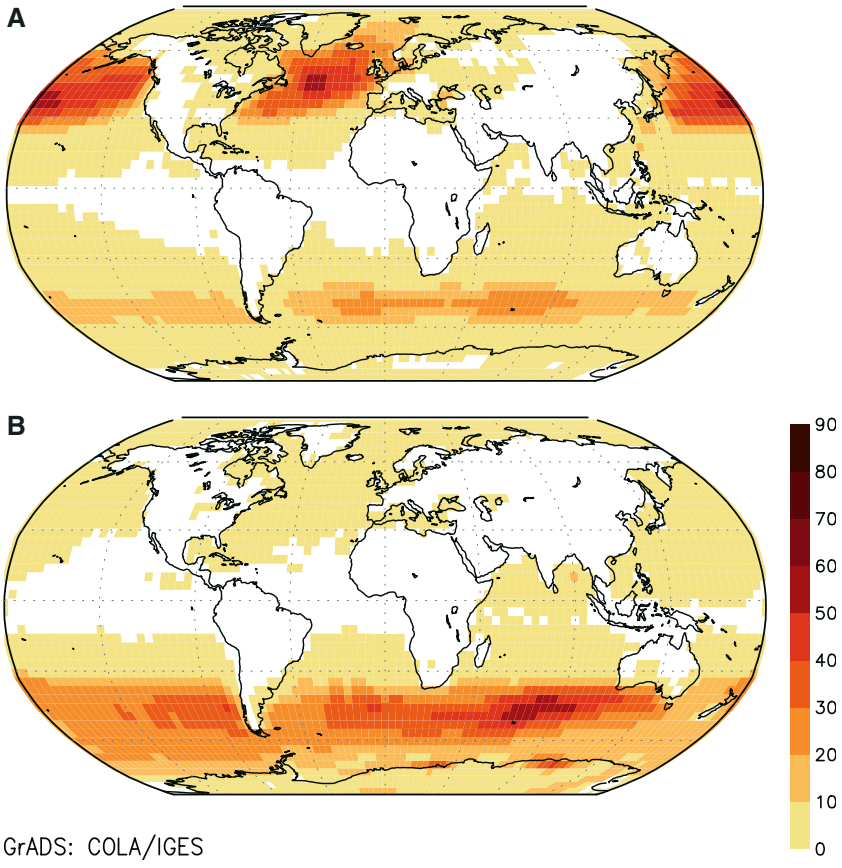

Fig. 1 Frequency of storm days (number of days with maximum daily 10 m wind speed reaching or exceeding the lower threshold of 8 Bft) for **a** DJF and **b** JJA for the pre-industrial period 1551–1850 in the historical experiment H2

mainly on the occurrence of storm days. A corresponding analysis of simulation H1 shows that the storm climate of both simulations hardly differs.

The graphical representation of storm day frequency for the industrially influenced period 1851–1990 in H2 is given in Fig. 2a and b. A comparison with the respective pre-industrial maps (Fig. 1a, b) exhibits no noticeable difference. For a better comparison, Fig. 2c and d show the differences between industrial and pre-industrial periods for both winter seasons. They are negligible. If we compare 1851–1990 with the recent period 1961–1990 too, no noticeable difference can be seen (not shown). The same analysis has also been performed for severe storm days (not shown), exhibiting no apparent differences also.

In a next step we analyze the control run N, in order to investigate the frequencies of extreme wind speed events in an undisturbed simulation under contemporary GHG conditions. The 1,000 year long time series of maximum 10 m wind speed is divided into three independent periods of 300 year length each (year 1–300, 351–650 and 701–1,000). As we expect, the storm activity does not change from period to period. Compared to the maps for the pre-industrial and industrially influenced periods of H1 and H2, only a slight difference is suggested, namely a poleward shift of the region with maximum frequency on both hemispheres in the control run (not shown). This is due to the constant present-day GHG concentration as a forcing factor in N, which is lacking in the pre-industrial period in H2. Since during the industrially influenced period the GHG concentrations first have to increase until they reach present-day conditions, the increase simulated for the most recent past has not yet had an effect on the time mean.

Finally, we analyze the wind data of the climate change experiments CMIP2, A2 and B2 in the same way. Compared to N, H1 and H2 for the northern winter season, the region in the North Atlantic Ocean with the largest number of storm days per season (50–60 as well) has enlarged in all three future scenarios. As in N, this region is shifted to the northeast, which can be seen exemplarily for A2 in Fig. 3a. This is obviously due to the marked rise of GHGs in the climate change experiments. An increase of storm day frequency also occurs in the region of the Southern Ocean storm track for JJA, which is notorious for prevailing strong and ubiquitous westerly winds since they are not impeded by large land areas like the winds in the NH. Here, the maximum number of storm days per season is about 60–70 over the South Indian Ocean (Fig. 3b), i.e. about 20% more compared to the pre-industrial time periods of H1 and H2. In contrast to Fig. 2c and d, where no difference between industrial and pre-industrial can be seen, the

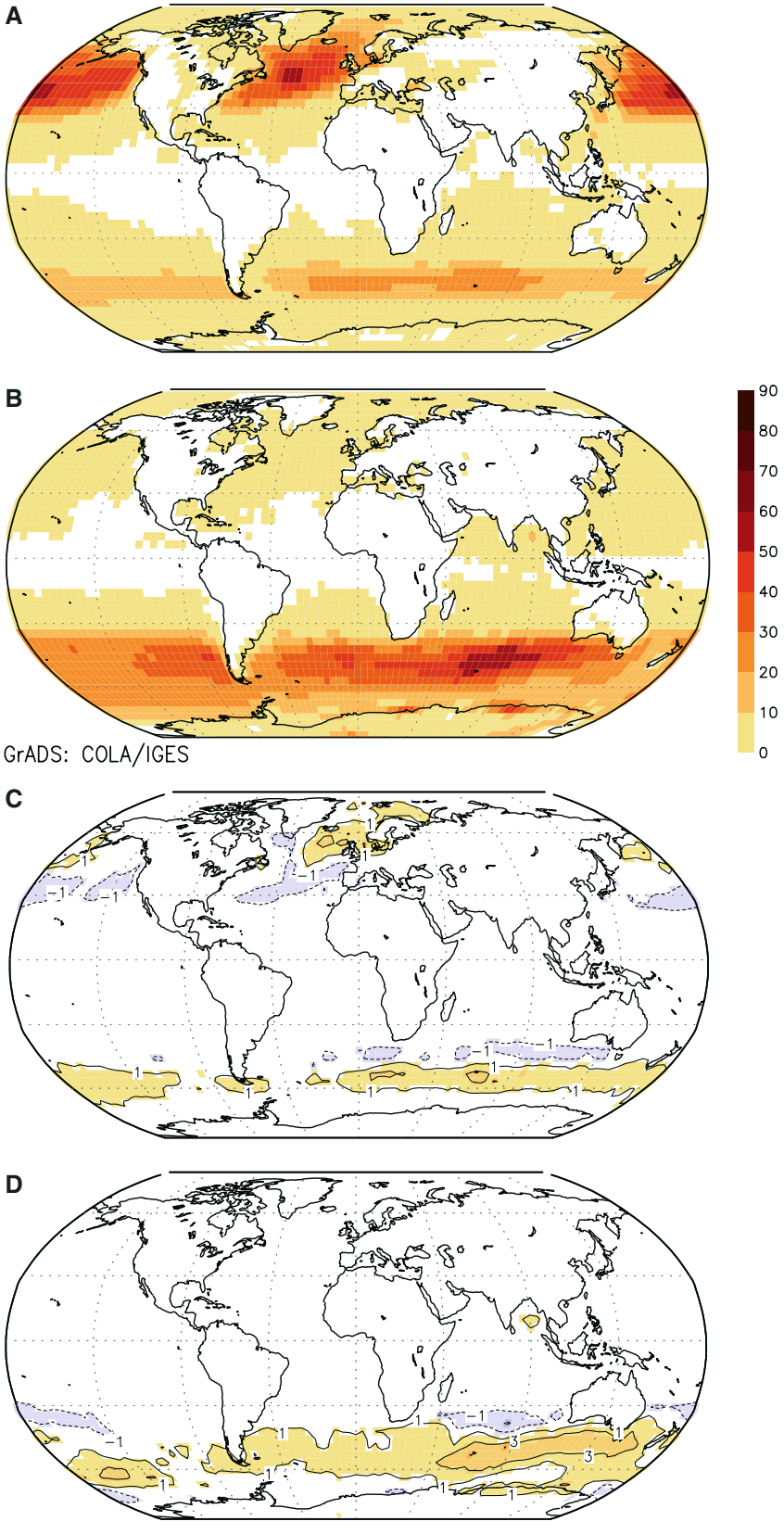

Fig. 2 *Upper two panels*: frequency of storm days for **a** DJF and **b** JJA for the industrially influenced period 1851–1990 in the historical experiment H2. *Lower two panels*: differences in storm day frequency between industrial and pre-industrial period of H2 for **c** DJF and **d** JJA

comparison between A2 and pre-industrial times (Fig. 3c, d) clearly exhibits regions with increases and decreases. Obviously, there is a poleward shift of the regions with high storm day frequencies on both hemispheres with future warming. This can be explained by the change in temperature gradients and sea surface

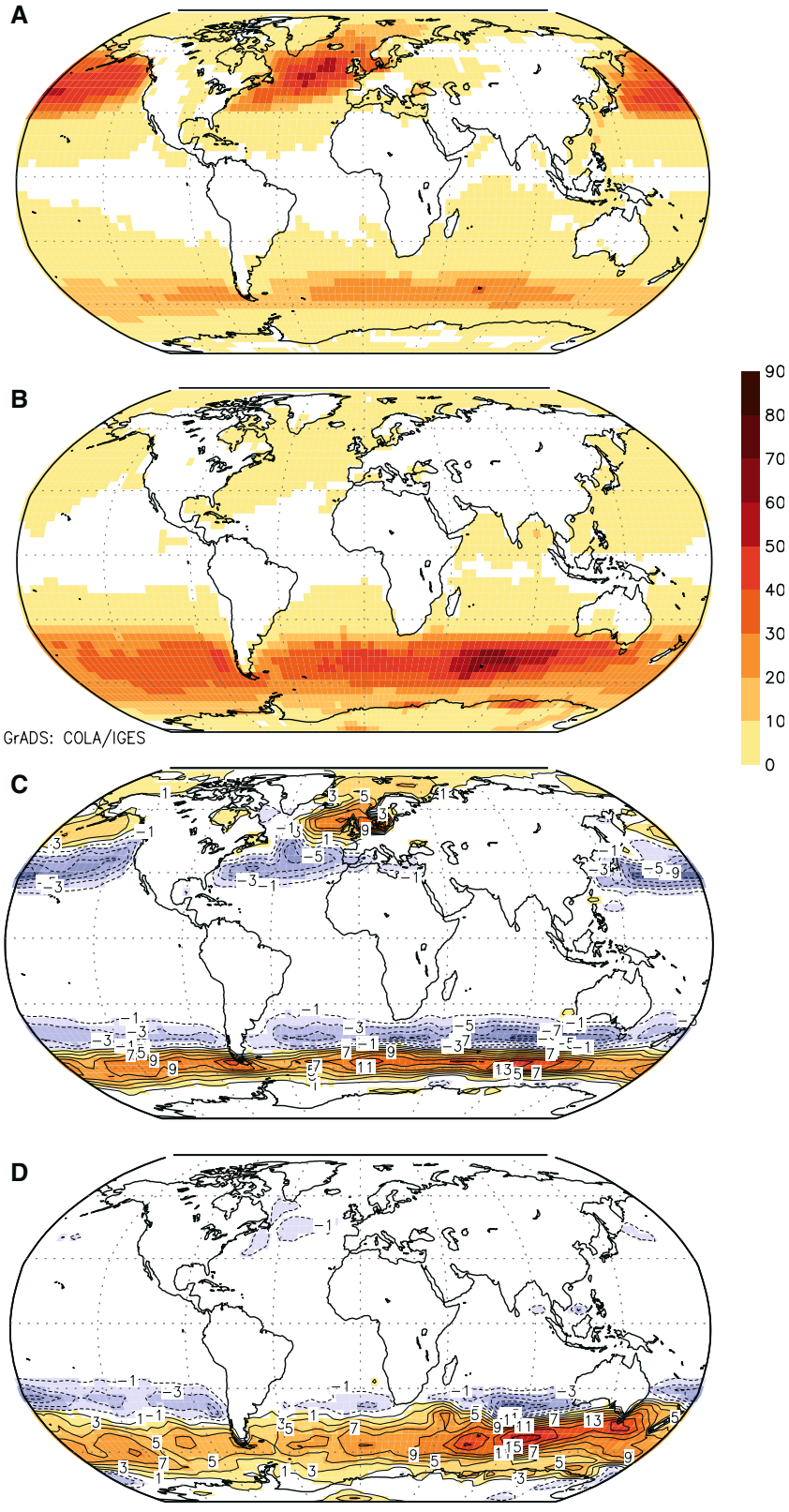

Fig. 3 *Upper two panels*: frequency of storm days for **a** DJF and **b** JJA for the climate change experiment A2. *Lower two panels*: differences in storm day frequency between climate change experiment A2 and pre-industrial period of H2 for **c** DJF and **d** JJA

temperature and the withdrawal of the ice edges in a warmer climate, causing a poleward shift of the regions of cyclogenesis and the whole storm track.

In order to assess what the threshold of 8 Bft actually relates to in the "real world", a comparison of the modelled storm day frequencies with those obtained by

applying our method to NCEP/NCAR or ERA-40/ECMWF reanalysis data could be considered. But such a comparison is not appropriate for the following reasons: (1) The reanalysis databases do not provide instantaneous maximum 10 m wind speeds as have been analysed here. (2) The 10 m wind speed (which also could be useful for comparison) in our model version is available as an average over the output interval (12 h) only, whereas reanalysed winds are instantaneous. We therefore refer to the findings of Weisse et al. (2005), who have analysed the storm climate of the Northeast Atlantic and the North Sea simulated by a regional climate model and compared their results with observations of marine stations. They show that their model is able to reproduce the numbers of moderate and severe storms realistically. From there we assume that the frequency of storms days determined by our method reflects a realistic storm climate.

Figure 4 shows the mean positions (averaged over ten winter seasons) of the grid points where the storm frequency is maximum as functions of time. The time series are displayed for the pre-industrial and industrially influenced period in H2 and A2 for all three oceans. Additionally the long time average of longitude and latitude has been indicated as a straight line to make it easier to identify trends. In the pre-industrial and industrial periods, the latitudinal and longitudinal positions in the North Atlantic Ocean hardly change, since the time series show no trend and the variability is low (Fig. 4a, upper four panels). This is similar to the latitudinal position in the Southern Ocean, whereas the corresponding longitudinal position changes slightly from 1551–1850 (Fig. 4c, H2 pre-industrial). This feature is even more outstanding in the Pacific region (Fig. 4b), where the longitudinal position jumps back and forth between 145 W and 175 E with SDs much higher than in the other regions. In the Pacific Ocean in all three time periods the longitudinal and latitudinal positions are dispersed over a large region. With rising GHG concentrations (future scenario A2), the positions tend to migrate further poleward in all oceans. Similar results can be found for H1 and CMIP2 (not shown). However, the longitudinal positions in H1 are moving a little more back and forth over the years than in H2.

A simple approach to define a storm index for frequency is to determine the mean number of storm days in winter per grid point for each hemisphere. For the NH this index is nearly the same for all simulation periods, i.e. there is no increase of modeled NH storm frequency with increasing GHGs. For the SH, however,

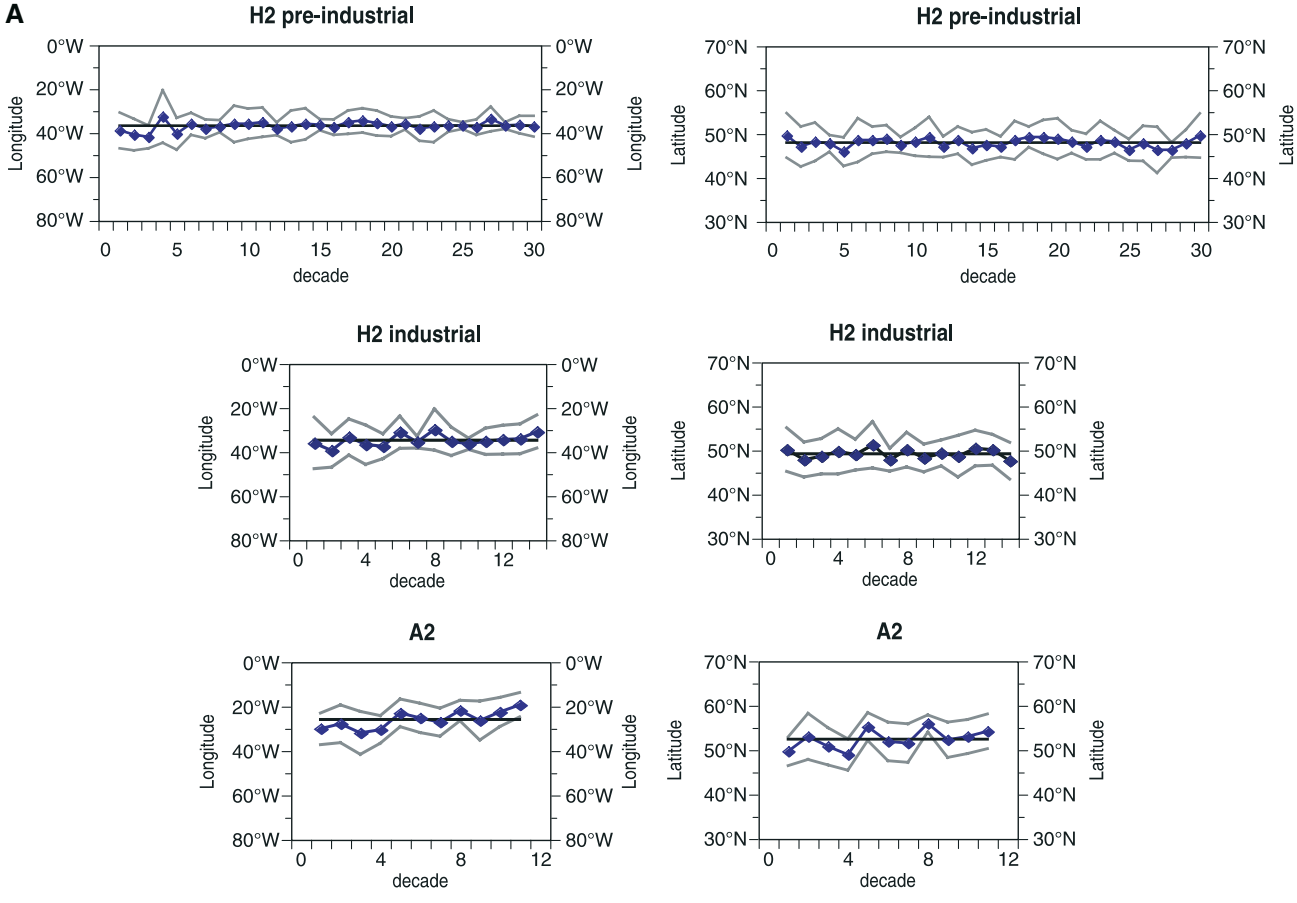

Fig. 4 Mean positions of the storm frequency maximum in H2 (pre-industrial and industrially influenced period) and A2 in the **a** North Atlantic, **b** North Pacific and **c** Southern Ocean region. The time series represent the positions in terms of mean longitude and latitude averaged over ten winter seasons. The *black line* shows the long time average, the *gray lines* indicate the SD

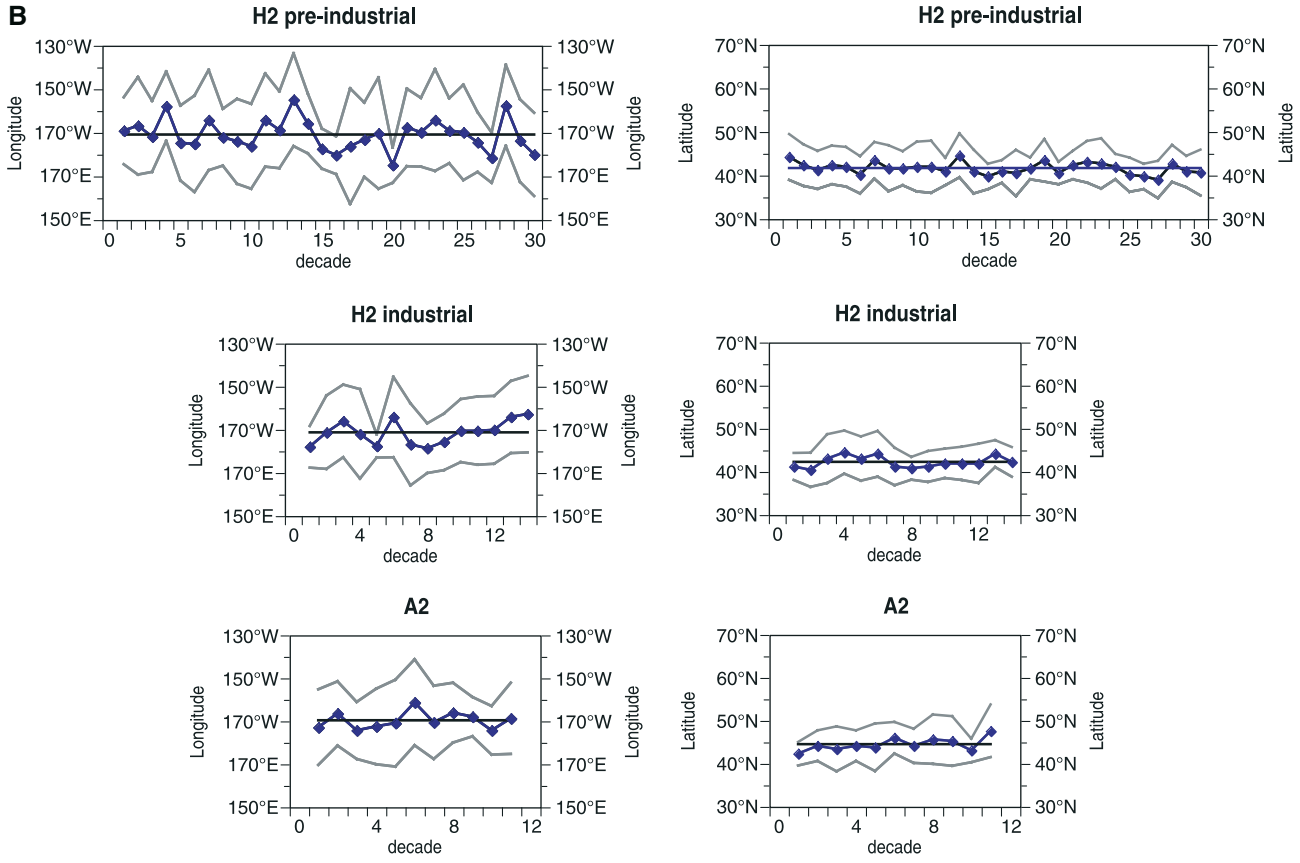

this index indicates an increase of modeled SH storm frequency beginning with industrialization (Fig. 5a, b). The NH and SH indices differ in magnitude, because the NH has more land points, where the winds are slowed down, than the SH. If this index is displayed as a function of time for each hemisphere, the SH trend can be seen still more clearly. This is shown exemplary for the pre-industrial and industrial phase of H2 and for A2 in Fig. 5c, with SDs of 0.36 (NH) and 1.13 (SH).

The same index determined separately for the North Atlantic (90 W–30 E) and North Pacific region (150 E–90 W) however, shows an increase in total number of storm days for the North Atlantic Ocean, but a decrease for the North Pacific Ocean (Fig. 5d–f). The SDs of the index time series in Fig. 5f are 0.84 (North Atlantic), and 0.67 (North Pacific). The slight North Pacific decrease in storm frequency can be confirmed with Fig. 3c, which shows that the region of decrease over the North Pacific Ocean is larger than that of increase.

5 Dominant modes of storm variability—storm shift index

We want to express the variations in storm climate in the three storm track regions by using the same reference frame. To do so, we first center all storm frequency data of H1 plus CMIP2, H2 plus A2, and H2 plus B2, by subtracting the 1551–1850 pre-industrial mean of the H2 experiment (which is defined as our reference period). Secondly, we calculate the leading EOFs (Empirical Orthgonal Function) from the centered data of the pre-industrial H2 simulation. Finally, we project the centered 1551–2100 data from H2 plus A2, and H2 plus B2, onto these EOFs. (With EOFs we refer to the spatial structures, while the corresponding "principal components" (PCs) reflect their development in time.) The same projection is applied with the centered 1551–2150 data from H1 plus CMIP2. The resulting PC time series are considered as our winter storm shift indices for the North Atlantic, North Pacific and Southern Ocean. They are also standardized to unit variance for the pre-industrial time. Since these numbers are calculated with the same reference means and patterns, the storm shift indices may be compared among the different simulations.

The first pre-industrial EOFs of H2 for the North Atlantic, North Pacific and SH region are shown in Fig. 6 (left column, top to bottom). The spatial structures of these EOFs reflect a shift of the area with maximum storm activity. The EOFs represent 23.4%, 26.5% and 11.2% of the total simulated variance. Are these patterns of storm frequency, characterizing a climate undisturbed by human activities, also the crucial patterns for describing the future climate? To assess this, as an example we calculate the linear trend of storm frequency at each grid point for the most extreme scenario A2. A plot of the slope coefficient for the three regions generates the patterns shown in Fig. 6 (right

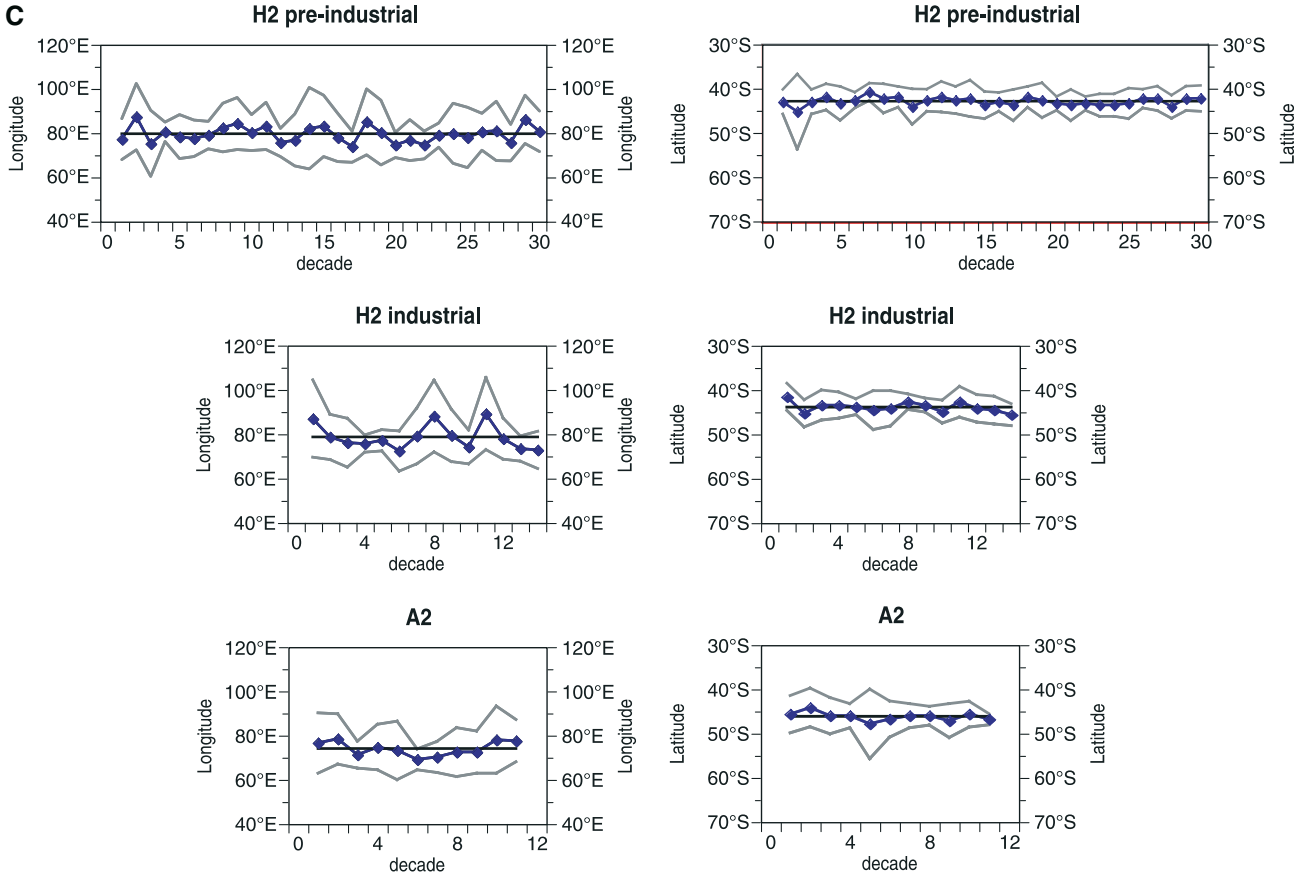

column, top to bottom). As we expect from our previous results, over the North Atlantic and in the SH, the regions with the strongest increasing trends extend over a larger area than those with the strongest decreasing trends. Over the North Pacific Ocean, however, it is the opposite way round. Since the first pre-industrial EOFs show a relatively good correspondence with the slope coefficient patterns, we conclude that these EOFs can also describe the future climate in terms of storminess.

For the North Atlantic Ocean however, the correlation is not perfect, since the region of maximum slope coefficient is located more eastward than the maximum of the first EOF. If we examine also EOF2 to 5, the fourth EOF seems to describe this feature best. Moreover, the corresponding PC_4 time series exhibits the second largest SD of the first five PCs and, in addition, the largest signal-to-noise ratio (here defined simply by dividing the last value (at year 2100) by the SD). EOF4 and the five PC time series corresponding to the first five EOFs (determined by projection of the 1551–2100 data from H2 plus A2 on this EOF) are shown in Fig. 7. For the sake of briefness, EOF2, 3 and 5 are not shown. Even though EOF4 is of secondary importance for the pre-industrial period (describing only 6.1% of the total variance), it could also be considered when describing the future change for the North Atlantic region. However, to simplify matters, we only take into account the first EOFs in the following.

Both storm indices—for frequency and shift—versus the near surface temperature averaged over the respective regions are displayed in Fig. 8 for the North Atlantic Ocean, North Pacific Ocean and SH. The temperature–time series are standardized in the same manner, namely such that, during the H2 pre-industrial reference period, the mean is zero and the SD is one. We show results for experiment H1 continued with CMIP2 (Fig. 8a–c) and H2 continued with A2 and with B2 (Fig. 8d–f). With both sets of experiments we achieve similar results: in pre-industrial times the storm indices are almost stationary and decoupled from temperature. There is possibly a very minor upward trend, which, surprisingly, does not match the trend in temperatures emerging since the beginning of the industrialization in the middle of the nineteenth century. The future climate experiments begin with a storm variability level that is consistent with the level in the historical experiments. But this level increases clearly in the 21st century—in parallel with the development of temperature, with the exception of the storm frequency index in the North Pacific region.

For the North Atlantic Ocean, there is a future poleward shift of the region with highest storm frequency beginning with the industrialization and overall a slight increase in storm frequency. For the North Pacific region, the result is a poleward shift but overall, a decrease in storm frequency. The result for the SH is a

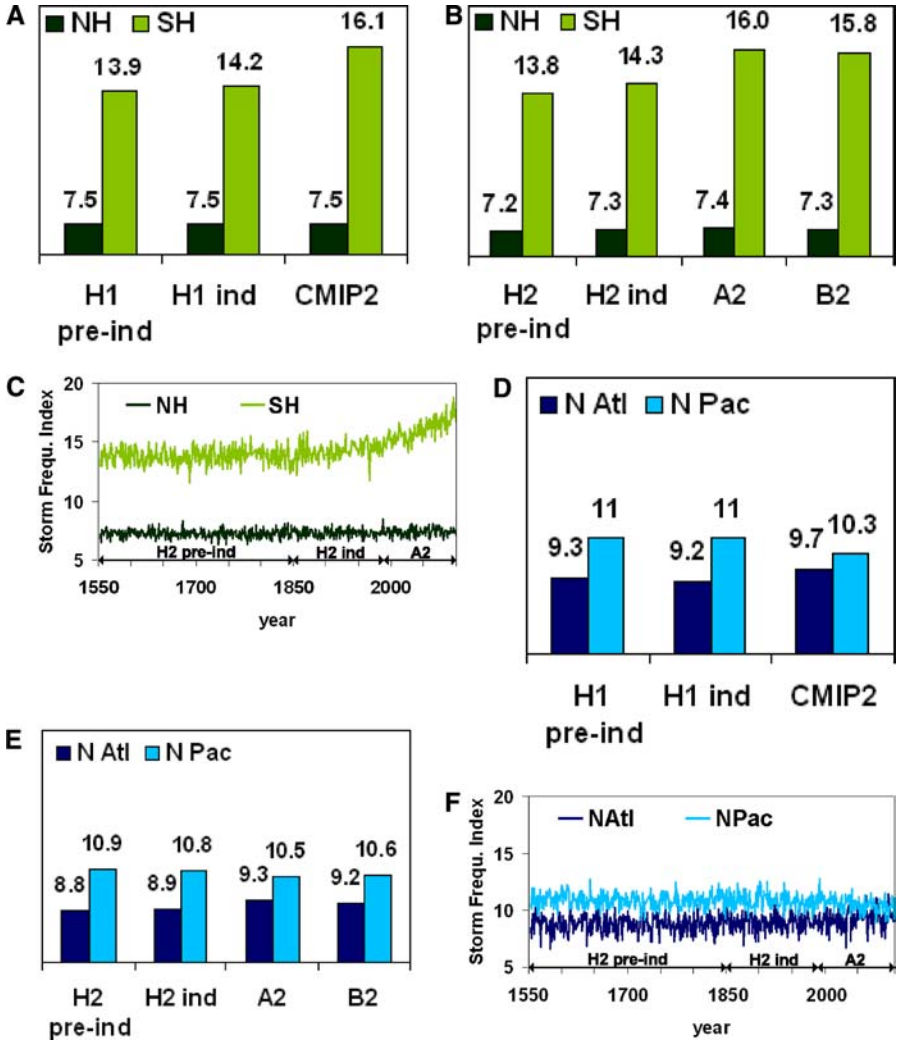

Fig. 5 **a** Storm frequency index defined as the mean number of storm days in winter per grid point averaged over the pre-industrial and industrially influenced periods of H1 and over the climate scenario CMIP2 for each hemisphere. **b** As in (**a**) but for H2 and A2 respectively B2. **c** Index as function of time corresponding to **b**, but only for H2 and A2. **d–f** As (**a**)–(**c**) but for North Atlantic region (90 W–30 E) and North Pacific region (150 E–90 W)

clear shift beginning with industrialization and overall, a large increase in storm frequency. These results apply for all three sets of experiments.

When we consider the pre-industrial 2σ-range (horizontal gray lines in Fig. 8) as a normal within which climatic variations would remain most of the time as long as anthropogenic factors do not have a significant impact, then the simulated temperature conditions are no longer "normal" from the 1950s for the North Atlantic and North Pacific, and from about 1990 on the SH. The storminess signals for the North Pacific, however, emerge some decades later, at about the year 2000.

The storm activity on both hemispheres is closely related to the simulated arctic oscillation (AO) and antarctic oscillation (AAO) indices, defined as the PCs corresponding to the first EOF of the NH and SH mean sea level pressure (mslp), respectively. Fig. 9a–d shows the AO and AAO patterns for the pre-industrial period of H2 and the A2 scenario. A clear shift of the centers of action to the east with future warming in both the North Atlantic and the North Pacific region can be seen. This can be ascertained also by comparing the patterns of H1 pre-industrial and CMIP2 (not shown) and is analog to the NAO shift found by Ulrich and Christoph (1999). On the SH the pattern is elongating with the CO_2 increase. The multi-century time series of the AO and AAO indices are determined by projection of the 1551–2100 mslp data from H2 plus A2 on the pre-industrial EOFs for the NH respectively SH. On both hemispheres, the indices are highly correlated with our storm shift indices (NH: 0.92, SH: 0.96). On the NH the link between the AO index and the storm shift index is unchanged during all time periods, while on the SH the storminess grows faster than the AAO index during the twenty-first century (Fig. 9e, f).

6 Discussion

The major results of our study are that

1. During historical times, storminess on both hemispheres is remarkably stationary with little variability.

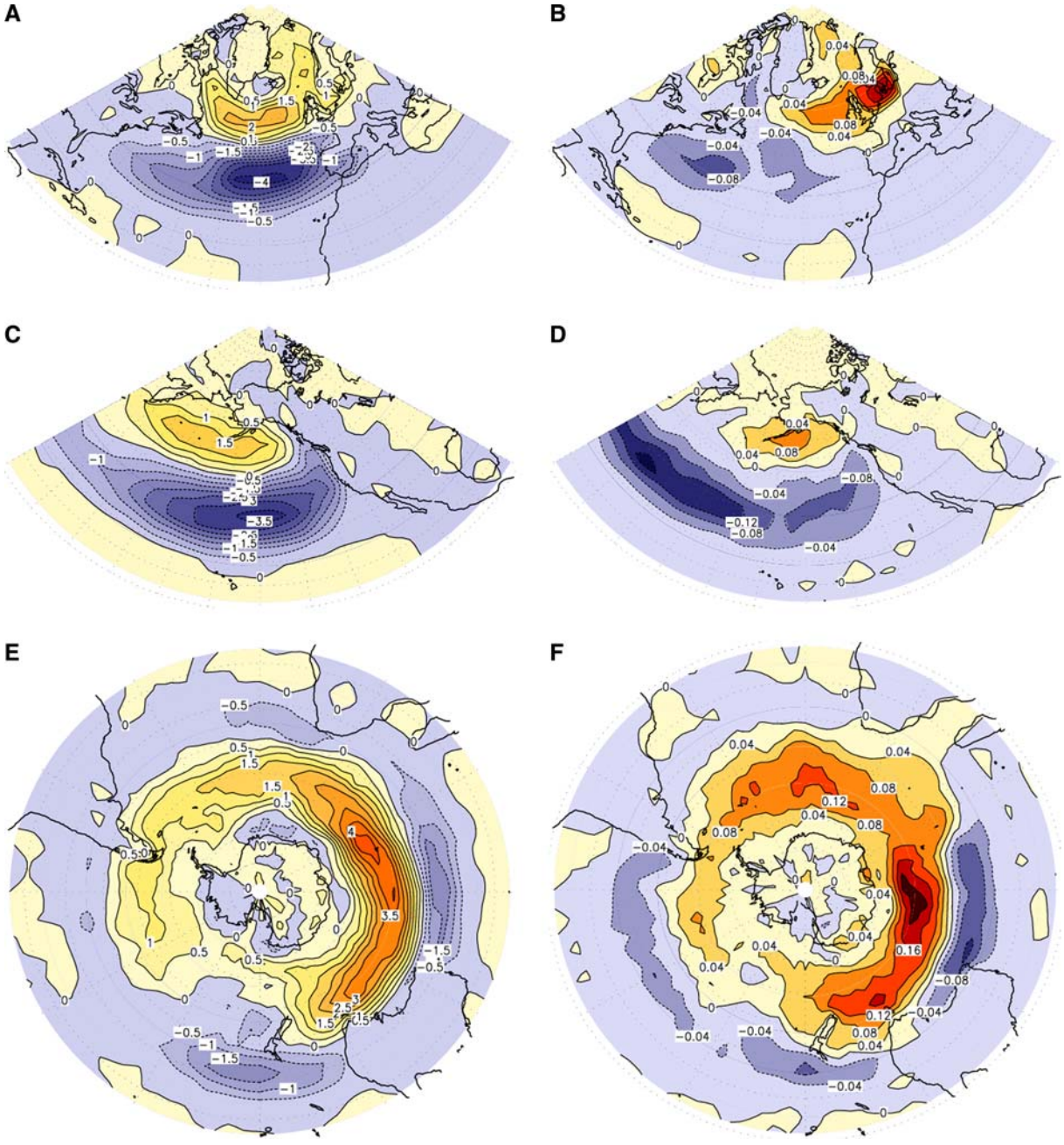

Fig. 6 a, c, e Leading EOFs of storm frequency for the pre-industrial period of experiment H2 for the North Atlantic, North Pacific and SH region. **b, d, f** Corresponding patterns of linear slope coefficient displayed at each grid point for the climate change experiment A2 determined by a linear trend analysis

2. During historical times, storminess and large-scale temperature variations are mostly decoupled.
3. In the climate change scenarios, with a strong increase of GHG concentrations, in the North Atlantic and Southern Ocean both temperature and storm shift indices rise quickly beyond the 2σ-range of pre-industrial variations, although the trends in the storms are smaller than the trends in temperature. In the North Pacific, moreover, the changes in storms tend to occur after the changes in temperature.
4. There are indications for a poleward shift of the regions with high storm frequency in both hemispheres with future warming. Altogether, we have ascertained an increase in the North Atlantic and SH storm frequency indices, whereas the North Pacific storm frequency index decreases with future warming.

The first result is consistent across the two historical simulations, but the second conclusion is not that straightforward. Indeed, in one of the two historical

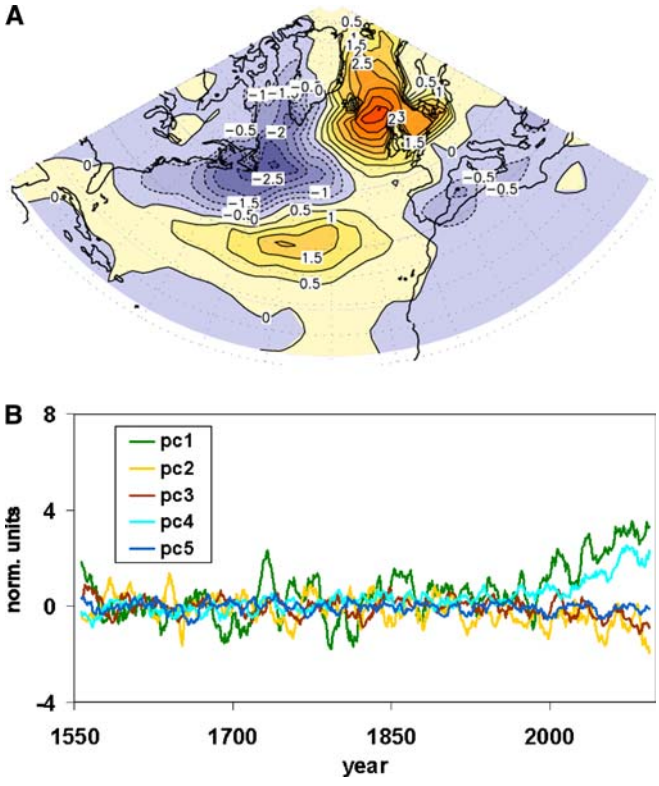

Fig. 7 **a** Fourth EOF of storm frequency for the pre-industrial period of experiment H2 for the North Atlantic region. **b** PC time series corresponding to the first five EOFs. The time series have been low pass filtered by computing an 11-year running mean and standardized to unit variance and zero mean in the pre-industrial period of H2

simulations (H1), during the two periods with extremely low external forcing, the Late Maunder Minimum (LMM, AD 1675–1710) and the Dalton Minimum (AD 1790–1840), a certain connection between storm track variability and temperature emerges over the North Atlantic Ocean (Fischer-Bruns et al. 2002; Zorita et al. 2004): during the first half of the LMM and the Dalton Minimum, less storms develop, while during the second half more storms pass across the North Atlantic Ocean. This feature is, however, not present in the H2 simulation, which has been run with the same forcing as H1. As it happens twice in H1, but not in H2, it may be seen as a random pattern. But it could also mean that a presently available larger ensemble of simulations may exhibit regime-like behavior.

Even if under certain circumstances a complex temperature-storminess link like the one described above in H1 is in operation, there is no evidence of a linear co-variability between extra-tropical storminess and large-scale temperature variations during historical times in our simulations. The fact that parallel trends emerge in the scenario simulations may be due to a casual relationship between warming and baroclinic instability, or may possibly be caused by, or at least be related to, the speed of temperature change. The latter hypothesis is supported by a result of Stone et al. (2001), who found the initial AAO intensification in the Geophysical Fluid Dynamics Laboratory (GFDL) CGCM to diminish after stabilization of the temperature change. The former would be supported if the warming were spatially inhomogeneous with stronger warming at subtropical latitudes and a weaker warming at subpolar latitudes—leading to a stronger meridional temperature gradient. However, this was not found to be the case.

A review of the literature about the many different climate change experiments with global coupled models reveals a mixed outcome. On the one hand, some models indicate an intensification of the North Atlantic storm track (such as Ulbrich and Christoph 1999; Knippertz et al. 2000; Andersen et al. 2001; Carnell et al. 1996). Knippertz et al. (2000), for example, relate the increase of cyclone activity in their simulation to increased upper tropospheric baroclinity and the increasing number of strong wind events to the increasing number of deep lows. On the other hand some studies find little change or even a reduction of extreme winds for the North Atlantic region (such as Beersma et al. 1997; Kharin and Zwiers 2000; Zwiers and Kharin 1998). An overview of several publications can be found in the IPCC Third Assessment Report (2001). As has been outlined there, Carnell and Senior (1998) performed an analysis of an ensemble of four future climate change experiments with rising CO_2 and sulfate aerosols and show that the number of weaker storms is reduced. They assume the reason for a weakening of storms in the future climate can be seen in the higher warming at higher latitudes compared to the warming at lower latitudes. As a consequence, the mean meridional temperature decreases, and fewer storms occur. Sinclair and Watterson (1999) find similar changes for both hemispheres. They emphasize that vorticity as a measure for cyclone strength does not increase. Finally, some sensitivities have been noticed (J.C. Fyfe, personal communication). One such result is that the Canadian Centre for Climate Modelling and Analysis (CCCma) model CGCM2 produces a much smaller AAO intensification than the model version CGCM1—with a different ocean mixing scheme being the only difference (Stone and Fyfe 2005). The other is the observation that also, the change of the southern storm track in different models depends on whether flux correction is invoked or not (J.C. Fyfe, personal communication).

Thus, the projection of our simulation is consistent with some simulations, but again inconsistent with others.

Obviously there is one significant caveat with our study: it is also just a result of a single model. Even though models might be powerful in reproducing many non-trivial aspects of climate—they may all be too simple or suffer from similar inconsistencies making them inadequate positive analogs of the real climate system. Moreover only single simulations of each scenario have been used. However, there is no

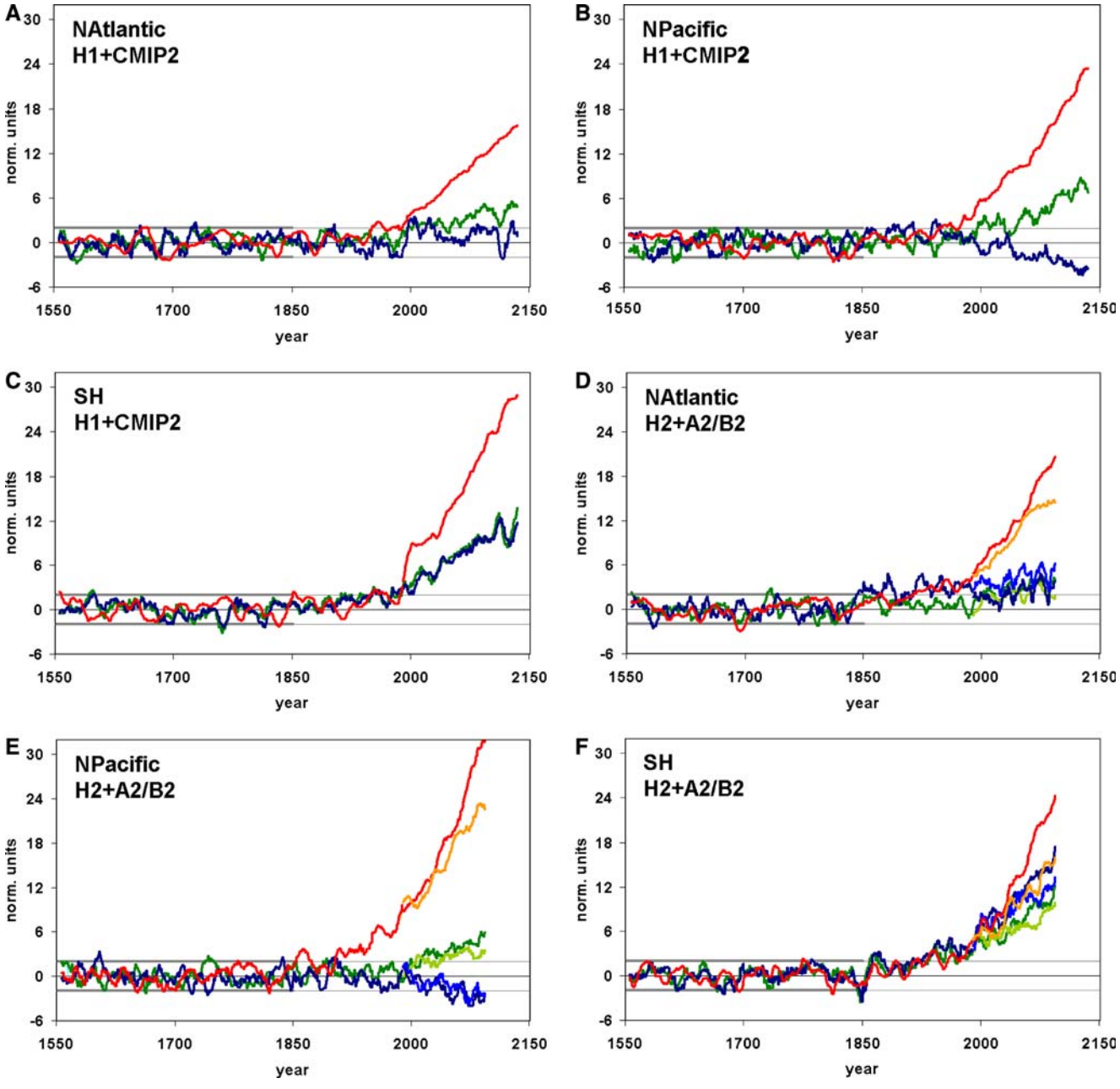

Fig. 8 Mean near-surface temperature (*red*/*orange colors*), storm frequency index (*blue colors*) and storm shift index (*green colors*) for North Atlantic, North Pacific and Southern Ocean (*from top to bottom*) in different experiments. **a–c** H1 (until 1990) and CMIP2 (after 1990). **d–f** H2 (until 1990) and two SRES scenarios (after 1990): A2 (red, dark blue and dark green) and B2 (orange, light blue and light green). The bold gray lines indicate ±2 SDs for the pre-industrial period of H2, continuing as *thin gray lines*. All time series have been low pass filtered by computing an 11-year running mean and standardized to unit variance and zero mean in the pre-industrial period of H2

empirical evidence available to study hypotheses like the one examined by us. Therefore, there is no alternative to the use of quasi-realistic models, but the caveat needs to be kept in mind (Müller and von Storch 2004).

Acknowledgements This work was partially funded by the 'Sonderforschungsbereich' (SFB) 512 sponsored by the 'Deutsche Forschungsgemeinschaft' (DFG) and by the KIHZ project of 'Helmholtz-Gemeinschaft Deutscher Forschungszentren e.V.' (HGF). The ECHAM4/HOPE-G was provided as community model by the Model & Data Group at the Max-Planck Institute for Meteorology. The model simulations have been integrated at the DKRZ climate computing center. We thank Reiner Schnur for helpful suggestions. Discussions with John Fyfe and George Boer were constructive and helpful as well. We gratefully acknowledge the help of Norbert Noreiks in adapting some of the figures.

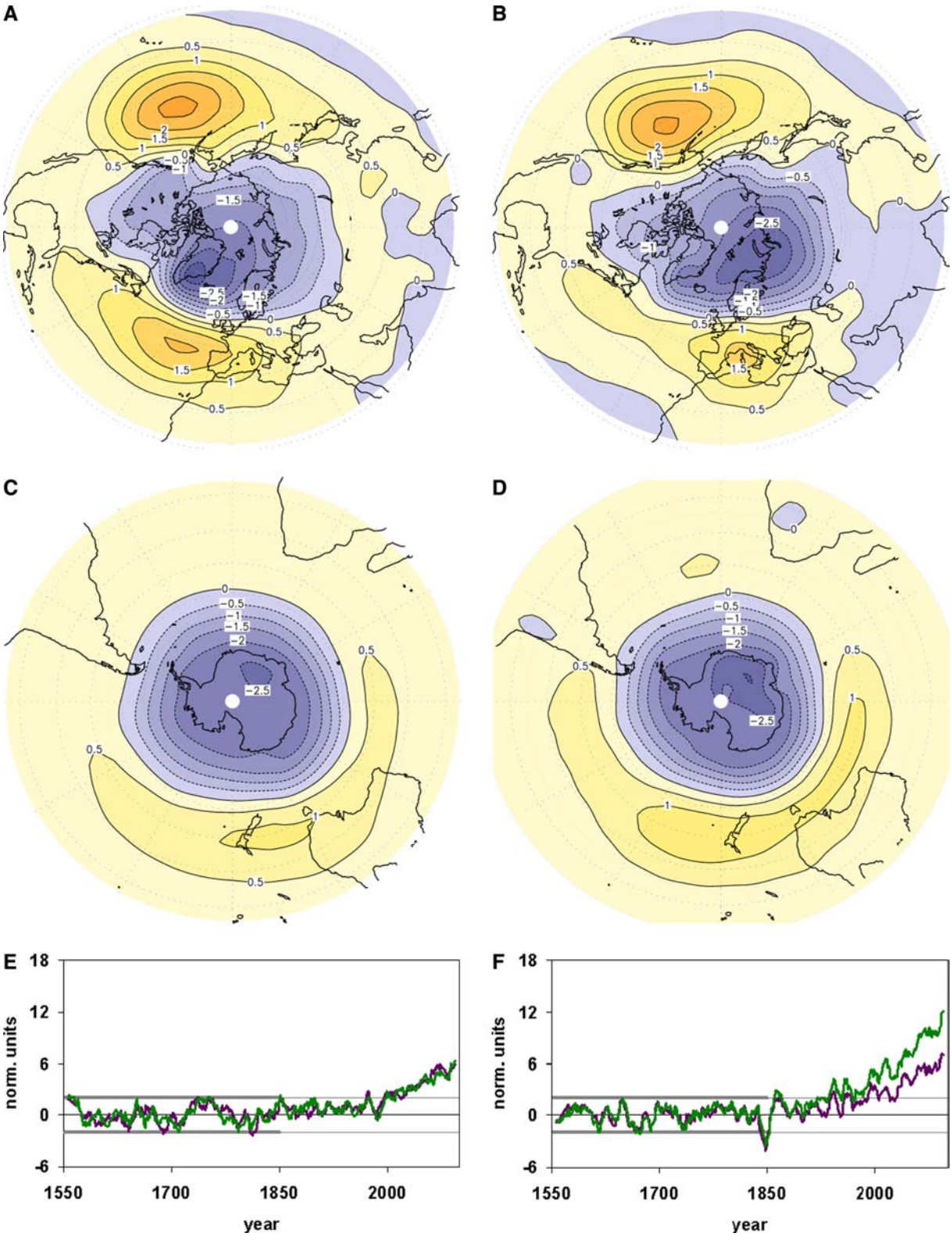

Fig. 9 **a** AO pattern, defined as the first EOF of NH mslp for the pre-industrial period of H2. **b** as in (**a**) but for A2. **c, d** as in (**a**) and (**b**) but SH AAO pattern. **e** AO index (*purple*) and NH storm shift index (*green*). **f** AAO index (*purple*) and SH storm shift index (*green*). For explanation of *gray lines* and filtering see Fig. 8

References

Alexandersson H, Schmith T, Iden K, Tuomenvirta H (2000) Trends of storms in NW Europe derived from an updated pressure data set. Clim Res 14:71–73

Andersen, UJ, Kaas E, May W (2001) Changes in the storm climate in the North Atlantic/European region as simulated by GCM timeslice experiments at high resolution. Danish Climate Centre Report, No 01-1, ISSN: 1399–1957 (Online), 15 pp

Bärring L, von Storch H (2004) Northern European Storminess since about 1800. Geophys Res Lett 31:L20202. doi:10.1029/2004GL020441:1–4

Beersma JJ, Rider KM, Komen GJ, Kaas E, Kharin VV (1997) An analysis of extratropical storms in the North Atlantic region as simulated in a control and 2'CO2 time-slice experiment with a high-resolution atmospheric model. Tellus 49A:347–361

Carnell RE, Senior CA, Mitchell JFB (1996) An assessment of measures of storminess: Simulated changes in Northern Hemisphere winter due to increasing CO_2. Clim Dynam 12:467–476

Carnell RE, Senior CA (1998) Changes in mid-latitude variability due to increasing greenhouse gases and sulfate aerosols. Clim Dynam 14:369–383

Crowley T (2000) Causes of climate change over the past 1000 years. Science 289:270–277

de Kraker AMJ (1999) A method to assess the impact of high tides, storms and storm surges as vital elements in climate history. The case of stormy weather and dikes in the Northern part of Flanders, 1488–1609. Clim Change 43:287–302

Fischer-Bruns I, Cubasch U, von Storch H, Zorita E, Gonzáles-Rouco JF, Luterbacher J (2002) Modelling the Late Maunder Minimum with a 3-dimensional Ocean-Atmosphere GCM. CLIVAR Exchanges, No. 25 (vol 7, no 3/4), pp. 59–61. International CLIVAR Project Office, Southampton, UK, ISSN No. 1026–0471

Friedman RM (1989) Appropriating the weather. Vilhelm Bjerknes and the construction of a modern meteorology. Cornell University Press, 251 p. ISBN 0 8014-2062-8

González-Rouco JF, Zorita E, Cubasch U, von Storch H, Fischer-Bruns I, Valero F, Montavez JP, Schlese U, Legutke S (2003) Simulating the climate since 1000 A.D. with the AOGCM ECHO-G. In: Proceedings of the ISCS1 2003 symposium, 'Solar Variability as an Input to the Earth's Environment', Tatranská Lomnica, Slovakia, 23–28 June 2003. ESA SP-535, 329–338

IPCC (2001) Climate change 2001, the scientific basis. In: Houghton JT, Ding Y, Griggs DJ, Noguer M, van der Linden PJ, Xiaosu D (eds) Contribution of working group I to the third assessment report of the intergovernmental panel on climate change (IPCC). Cambridge University Press, UK, p 944

Kaas E, Li T-S, Schmith T (1998) Northeast Atlantic winter storminess 1875–1995 re-analysed. Clim Dynam 14:529–536

Kharin VV, Zwiers FW (2000) Changes in the extremes in an ensemble of transient climate simulations with a coupled atmosphere-ocean GCM. J Climate 13: 3670–3688

Knippertz P, Ulbrich U, Speth P (2000) Changing cyclones and surface wind speeds over the North Atlantic and Europe in a transient GHG experiment. Clim Res 15:109–122

Knippertz P, Christoph M, Speth P (2003) Long-term precipitation variability in Morocco and the link to the large-scale circulation in recent and future climate. Meteorol Atmos Phys 83:67–88

Lamb HH (1977) Climate: present, past and future, vol 2. Climatic history and the future. Methuen, London, 835 p

Legutke S, Voss R (1999) The Hamburg atmosphere–ocean coupled circulation model ECHO-G. Technical report no. 18, German Climate Computer Center (DKRZ), Hamburg

Legutke S, Maier-Raimer E (1999) Climatology of the HOPE-G global ocean—sea ice general circulation model. Technical report no. 21, German Climate Computer Center (DKRZ), Hamburg

Mann M, Bradley RS, Hughes MK (1998) Global-scale temperature patters and climate forcing over the past centuries. Nature 392:779–789

Meehl GA, Boer GJ, Covey C, Latif M, Stouffer RJ (2000) The Coupled Model Intercomparison Project (CMIP). Bull Am Meteorol Soc 81:313–318

Min SK, Legutke, Hense A, Kwon W-T (2004) Climatology and internal variability in a 1000-year control simulation with the coupled climate model ECHO-G. M&D Technical Report, No. 2, Max Planck Institute for Meteorology, Hamburg, Germany, 67pp (http://mad.zmaw.de/Pingo/reports/Te-Report_Web02.pdf)

Müller P, von Storch H (2004) Computer modelling in atmospheric and oceanic sciences—on building knowledge. Springer, Berlin Heidelberg New York, 304 p. ISN 1437-028X

Nakicenovic N, Swart R (eds) (2000) Emission scenarios. Special report of the intergovernmental panel on climate change (IPCC) on Emission Scenarios. Cambridge University Press, UK. (http://www.grida.no/climate/ipcc/emission/index.htm)

Raible CC, Blender R (2004) Northern hemisphere mid-latitude cyclone variability in different ocean representations. Clim Dynam 22: 239–248

Roeckner E, Arpe K, Bengtsson L, Brinkop S, Dümenil L, Esch M, Kirk E, Lunkeit F, Ponater M, Rockel B, Sausen R, Schlese U, Schubert S, Windelband M (1992) Simulation of the present-day climate with the ECHAM model: Impact of model physics and resolution. Report no. 93, Max-Planck-Institut für Meteorologie, Bundesstr 55, Hamburg

Roeckner E, Arpe K, Bengtsson L, Christoph M, Claussen M, Dümenil L, Esch M, Giorgetta M, Schlese U, Schulzweida U (1996) The atmospheric general circulation model ECHAM4: model description and simulation of present-day climate. Report no. 218, Max-Planck-Institut für Meteorologie, Bundesstr 55, Hamburg

Schmidt H, von Storch H (1993) German Bight storms analyzed. Nature 365:791

Sinclair MR, Watterson IG (1999) Objective assessment of extratropical weather systems in simulated climates. J Climate 12:3467–3485

Stendel M, Roeckner E (1998) Impacts of horizontal resolution on simulated climate statistics in ECHAM4. Report no. 253, Max-Planck-Institut für Meteorologie, Bundesstr 55, Hamburg

Stone DA, Weaver AJ, Stouffer RJ (2001) Projections of climate change onto modes of atmospheric variability. J Climate 14: 3551–3565

Stone DA, Fyfe JC (2005) The effect of ocean mixing parametrisation on the enhanced CO_2 response of the Southern Hemisphere midlatitude jet. Geophys Res Lett (in press)

Ulbrich U, Christoph M (1999) A shift of the NAO and increasing storm track activity over Europe due to anthropogenic greenhouse gas forcing. Clim Dynam 15:551–559

von Storch H, Stehr N (2000) Climate change in perspective. Our concerns about global warming have an age-old resonance. Nature 405:615

von Storch H, Zorita E, Jones J, Dimitriev Y, González-Rouco JF, Tett S (2004) Reconstructing past climate from noisy data. Science 306:679–682

WASA (1998) Changing waves and storms in the Northeast Atlantic. Bull Am Met Soc 79:741–760

Weisse R, von Storch H, Feser F (2005) Northeast Atlantic and North Sea storminess as simulated by a regional climate model 1958–2001 and comparison with observations. J Climate 18:465–479

Wolff J-O, Maier-Reimer E, Legutke S (1997) The Hamburg Ocean primitive equation model. Technical report, no. 13, German Climate Computer Center (DKRZ), Hamburg

Zinke J, von Storch H, Müller B, Zorita E, Rein B, Mieding HB, Miller H, Lücke A, Schleser GH, Schwab MJ, Negendank JFW, Kienel U, González-Ruoco JF, Dullo C, Eisenhauer A (2004) Evidence for the climate during the Late Maunder Minimum from proxy data available within KIHZ. In: Fischer H, Kumke T, Lohmann G, Flöser G, Miller H, von Storch H, Negendank JFW (eds) The KIHZ project: towards a synthesis of Holocene proxy data and climate models. Springer Berlin Heidelberg, New York, pp 397–414

Zorita E, Storch H, Gonzales-Rouco JF, Cubasch U, Luterbacher J, Legutke S, Fischer-Bruns I, Schlese U (2004) Transient simulation of the climate of the last five centuries with an atmosphere-ocean coupled model: the Late Maunder Minimum and the Little Ice Age. Meteorol Z 13:271–289

Zwiers FW, Kharin VV (1998) Changes in the extremes of climate simulated by CCC GCM2 under CO2-doubling. J Climate 11:2200–2222